Complex diagnostics of reactive glow discharges

Pavel Dvořák

Masaryk University, Faculty of Science
Department of Physical Electronics
Brno, Czech Republic

Abstract of PhD Thesis

Contents

Chapter 1

Introduction

Low-pressure capacitively coupled discharges have found their application in many branches of science and industry. They are used especially for the treatment of solid surfaces, i.e. plasma etching, depositions, ion implantation, the enhancement of surface energy, redox reactions etc. Moreover, they are used in the investigation of plasmochemical reactions or plasma crystals. Due to the recent discovery of the possibility to control independently the concentration of reactive species and the energy of ions impinging on a solid surface in dual frequency discharges, the capacitively coupled discharges are expected to be useful in yet more areas in the near future. Moreover, the capacitively coupled discharges are an interesting subject for research due to their nonisothermicity, several different mechanisms of plasma heating, nonlinearity of the volt-ampere characteristics, the variety of plasmochemical reactions that take place in the plasma and others.

This work focuses on the hydrogen discharge. Hydrogen plasma usually has a strong reduction and etching effects that are broadly used. Hydrogen discharges are used for the cleaning and etching of solid surfaces, reduction of rust on archaeological artefacts or oxides on semiconductors, passivation of defects by the manufacturing of thin silicon transistors, etc. It is worth mentioning the role of the hydrogen plasma in fusion or astrophysics. Hydrogen with admixtures is commonly used for the deposition of hard coatings. For example during the depositions of diamond or amorphous DLC films hydrogen etches the soft graphitic bonds and reacts with alkanes which produces reactive carbon containing radicals. Hydrogen discharges are also used as sources of ions for neutral beam injectors for fusion devices.

Though the low-pressure capacitively coupled hydrogen discharges represent an interesting subject for research, insuficent attention has been paid to their complex diagnostics, to date. Therefore the aim of this work is the diagnostics of the hydrogen capacitively coupled plasma. Chapter 2 describes the experimental arrangement and the sensitivity of the apparatus used. The basic results are briefly described in chapter 3. They are divided within one section refering to the visual appearance and electric characteristics of the discharge, several sections concerning the results obtained by means of several diagnostics methods (Langmuir probe, uncompensated probe for measurement of harmonic plasma potential components, reference probe, plasma process monitor, optical emission spectroscopy) and one section describing a model that explains the existence of two observed plasma modes. Chapter 4, briefly, concludes the results.

Chapter 2

Experimental

The experiments were carried out in a spherical (i.d. ca 33 cm) stainless steel reactor (fig. 2.1) with two horizontally mounted, parallel, stainless steel electrodes of 80 mm diameter. The upper electrode, embedded in a grounded ring, was driven at the frequency of 13.56 MHz. The bottom electrode was grounded. Their distance was 40 mm. The reactor was exhausted by a turbomolecular pump with a membrane pump. Prior to each experiment the reactor was pumped to pressure lower than 10^{-4} Pa.

The plasma parameters were measured as functions of the hydrogen pressure, vertical distance from the upper electrode (see fig. 2.1) and the RF power. The pressure varied within the range 1 – 200 Pa, RF power within the range 5 – 45 W. Under typical conditions the DC self-bias on the powered electrode was approximately -150 V demonstrating an asymmetric nature of the discharge due to grounded reactor parts. The RF voltage, the RF current and the self-bias were measured on the coaxial cable between the matching unit and the reactor.

The electron energy distributions (EEDs) were measured by the Langmuir probe (Scientific Systems Ltd.). The probe tip (length 1 cm, radius 0.19 mm) was placed at the discharge axis and its distance from the electrodes was changed. Passive compensation [1] of RF components of the plasma potential was used. The low-frequency changes of the plasma potential were measured and corrected by means of a reference probe [2]. The EEDs were obtained by the numerical calculation of the second derivative of the probe characteristics.

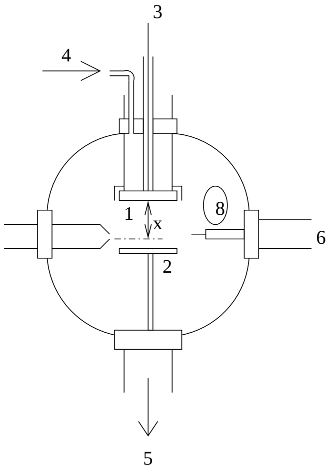

Figure 2.1: *Reactor scheme. 1 – upper electrode, 2 – bottom electrode, 3 – RF power supply, 4 – gas inlet, 5 – exhaust pumps, 6 – Langmuir probe, 7 – PPM, 8 – silica window, x is the "vertical distance" between the upper electrode and the PPM.*

The positive ion energy distributions (IEDs) were measured by Plasma Process Monitor PPM 421 (Balzers) consisting of an entry ion optics, a cylindrical mirror energy analyzer, a quadrupole mass filter and a secondary electron multiplier. The PPM was mounted parallell to the electrodes and its grounded extraction hood was 15 mm outside the space between the electrodes. The PPM was able to work only when the hydrogen pressure in the discharge chamber was lower than ca 4 Pa.

In order to estimate the energy dependence of the PPM sensitivity, the transmission of the entry ion optics had to be calculated. At first the critical angles for ions impinging on an orifice in the extraction hood were calculated. The critical angle is defined as the largest angle between the ion velocity and the optical axis of the entry optics enabling the ion to go through the entry optics into the energy analyzer. Ions impinging at angles larger than the critical angle cannot reach the energy analyzer and are captured by some of the electrodes in the entry optics. The critical angle depends on the kinetic energy of the ion (fig. 2.2). The transmission of the

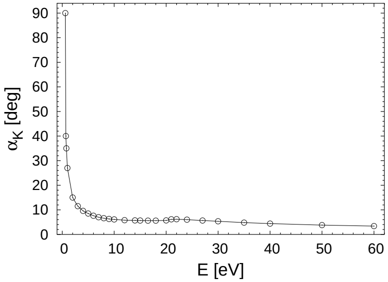

Figure 2.2: *The critical angle* α_K *as a function of the ion energy.*

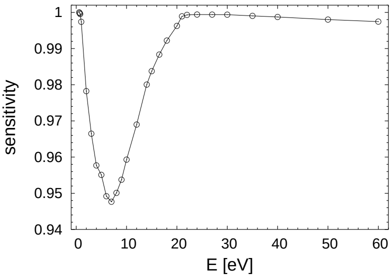

Figure 2.3: *The PPM sensitivity as a function of the ion energy.*

entry ion optics can be evaluated by integrating the ion angle distribution (IAD) up to the critical angle. Unfortunately, the IADs are not known. In order to find an approximate transmission function it was supposed that the ion velocity component perpendicular to the optical axis has Maxwell distribution. The ion temperature in the distribution was assumed to be 410 K that is equal to the rotational temperature of neutral gas measured by optical emission spectroscopy. This assumption was based on the fact that the kinetic energy of ions in the glow region of RF discharges is comparable to the temperature of neutral gas, because the ion plasma frequency is well below the RF frequency. The low value of the ion plasma frequency caused by the low ion density (approximately $10^7\,\mathrm{cm}^{-3}$) was confirmed by Langmuir probe measurements.

The calculated transmission function was in the entire measured energy range higher than 94 % (fig. 2.3), therefore the measured IEDs were not significantly distorted by the PPM. Nevertheless, the measured IEDs were corrected by means of the calculated transmission function. It is worth noticing that the assumptions above can lead to an underestimation of the perpendicular velocities and consequently to an overestimation of the transmission function.

The frequency spectrum of the plasma potential and the DC value of the floating potential were measured by means of an uncompensated probe made from a steel wire with diameter 0.25 mm. The unprotected section of the wire was 13 mm long, 83 mm of the wire were surrounded only by glass and the rest of the wire was also covered with brass (see fig. 2.4). The probe tip was, in a number of the measurements, located in the middle of the discharge volume.

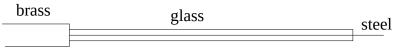

Figure 2.4: *The uncompensated probe.*

The probe was connected to a digital oscilloscope by a coaxial cable. The schema of the probe circuit is in the fig. 2.5. All the complex elements in the cascade matrix of the probe with the cable were estimated. It was possible to calculate the waveforms on the probe tip using this matrix. However, in order to calculate the waveforms in the plasma the capacity of the sheath at the probe had to be estimated. Therefore, the waveforms were measured with two different input impedances of the oscilloscope ($50\,\Omega$ and $1\,\mathrm{M}\Omega$). The current and the voltage on the probe tip were calculated in both cases. When it was assumed that the sheath at the probe behaves as an ideal capacitor and that the plasma potential was not affected by the oscilloscope impedance, it was possible to estimate the capacity of the sheath at the probe from the waveforms of the current and voltage on the probe tip.

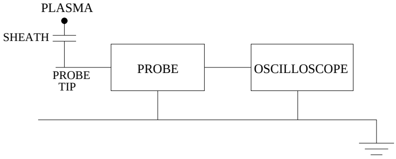

Figure 2.5: *The schema of the probe circuit.*

Unfortunately, this method of the sheath capacity estimation was not exact. The minimal value of the plasma potential amplitude can be estimated from the shape of the ion energy distribution that had been measured by means of the plasma process monitor. This value was a little higher than the value obtained by the presented measurements. This shows that the value of the sheath capacity was overestimated, which led to an underestimation of the harmonic amplitudes, especially with regard to the amplitude of the fundamental frequency. If the amplitudes were underestimated, the measured trends were not consequently devalued.

For the optical emission spectroscopy the spectrometer Triax 550 Jobin Yvon – Spex was used. The spectra were recorded through a silica window located in the half of the reactor height. The dependence of the spectrometer sensitivity on the wavelength is published in [3].

Chapter 3

Results

3.1 Electrical characteristics and visual appearance of the discharge

The high-frequency electrical characteristics of the discharge (RF voltage and current) measured on the coaxial cable between the matching unit and the reactor did not significantly depend on the hydrogen pressure. Their representative values are to be found in the table 3.1. In contrast to the RF characteristics, the absolute value of the self-bias on the powered electrode depended on the pressure having its maximum (180 V) between 10 and 15 Pa.

At low pressure (under 3 Pa) a thin, intensively radiating layer was observed at the edge of the sheath at the powered electrode. The sheath at the grounded electrode was so thin, that it was hardly recognizable with eye. The pressure increase led to the development of the sheath at the grounded electrode and to the increase of the luminosity of the bulk plasma. By further pressure increase (above 30 Pa) the centre of the discharge became dark and the brightness of the plasma-sheath boundaries intensified.

A sufficiently high increase of pressure or RF power led to an abrupt change of the discharge character. During this transition the sheath at the grounded electrode was strongly emphasized and the self-bias on the powered electrode decreased. The transition was observed also in nitrogen [4], oxygen and argon. Since the bulk plasma had a diffusive character

	unconfined mode			confined mode		
P [W]	V_{rf} [V]	I_{rf} [A]	$-U_b$ [V]	V_{rf} [V]	I_{rf} [A]	$-U_b$ [V]
10	86	1.9	84			
15	108	2.3	116			
20	124	2.7	141			
25	138	3.0	162	120	2.8	90
30	150	3.2	182	130	2.9	91
35	162	3.5	201	136	3.1	94
40	171	3.8	216	144	3.3	97
45	180	3.9	232	148	3.4	94

Table 3.1: *Amplitudes of the RF voltage (V_{rf}) and current (I_{rf}) and the self-bias on the powered electrode (U_b) at the pressure 10 Pa as functions of the RF power (P).*

before the transition while it was more confined between the electrodes after the transition, the mode that was stable at low pressure and power was termed "unconfined mode" and the mode stable at high pressure and power "confined mode". The transition showed hysteresis – when the confined mode was once achieved the discharge stayed in this mode even after certain decrease of the pressure or the RF power.

3.2 Langmuir probe measurements

The EEDs measured at low pressure (up to ca 7 Pa) had a simple Maxwellian shape. In other cases their shape was more complex and especially at high pressure or in the confined mode a presence of hot electrons group was also observed. The pressure dependences of the electron concentration (n_e) and the mean energy of electrons ($\langle E \rangle$) are shown in the fig. 3.1. The mean electron energy was correlated with the reciprocal value of the electron concentration, since the power delivered to one electron is approximately proportional to the value n_e^{-1}. The behaviour of the plasma potential was in agreement with the model published by Song et al. [5]. According to this model the steep decrease of the plasma potential between 2 and 10 Pa (see fig. 3.2) was caused, to a large extent, by the decrease in the electron

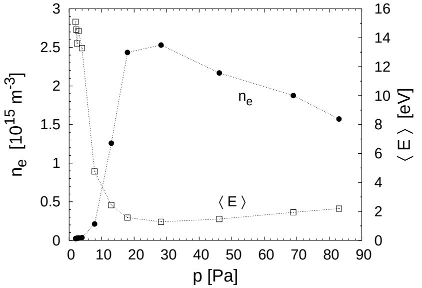

Figure 3.1: *The electron concentration n_e and mean energy $\langle E \rangle$ as functions of the pressure.*

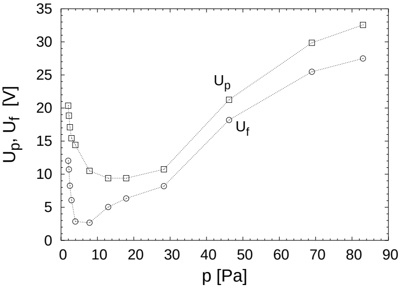

Figure 3.2: *The plasma potential U_p and the floating potential U_f as functions of pressure.*

energy.

At low pressure (2.5 Pa) the value of the electron concentration was relatively low (under $10^{14}\,\mathrm{m}^{-3}$) due to the high diffusion losses. The value of the electron concentration as well as the mean electron energy had sharp maxima at the boundary of the bulk plasma and the sheath at the powered electrode (fig. 3.3). The position of these maxima corresponded to the position of the radiating layer mentioned in sect. 3.1. The electron energy at the plasma-sheath boundary was unusually high, therefore the electrons penetrated into the sheath at the powered electrode, as can also be seen in fig. 3.3.

The pressure increase was followed by a steep increase of electron concentration, decrease of the mean electron energy and the bulk plasma became homogeneous (see fig. 3.4). Further increase in pressure (above 20 Pa) led to a slow decrease in electron concentration, increase of the plasma potential and to the change from nonlocal, to local character of the discharge.

During the transition from the unconfined to the confined mode the plasma potential (U_p) significantly increased (see fig. 3.5) and the sheath voltage at the powered electrode (U_a) decreased. As a result of the constant power delivered to the discharge the sum $U_p + U_a$ was not significantly changed by the mode transition. The asymmetry of the discharge, represented by the ratio U_a/U_p [6, 7, 8], was strongly reduced, as can be seen in fig. 3.6. Since the confined mode could not be sustained at the pressure

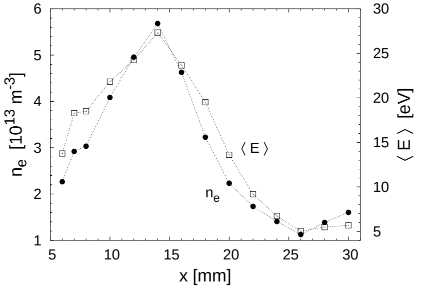

Figure 3.3: *The electron concentration and mean energy at 2.5 Pa as functions of the distance from the powered electrode (x).*

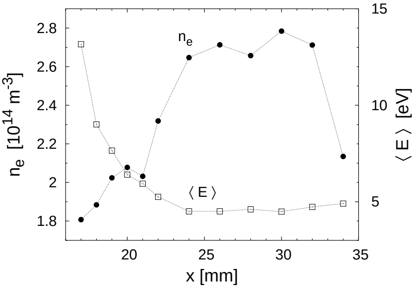

Figure 3.4: *The electron concentration and mean energy at 10 Pa in the unconfined mode as functions of the distance from the powered electrode.*

2.5 Pa, there are no results measured in the confined mode at this low pressure in the figures 3.5 – 3.8. The examples of the electron concentration and mean electron energy in the two modes are shown in fig. 3.7 and 3.8.

In the confined regime the plasma potential increased (fig. 3.5) and the discharge became symmetric (3.6) when the RF power was increased. On the contrary, in the unconfined mode the plasma potential and the electron energy were at times decreasing functions of the power. As can be shown by means of the equations published by Sobolewski [9], the decrease of the plasma potential is a result of discharge asymmetry, i.e. it is caused by the influence of the grounded reactor parts (walls and the shielding of the powered electrode).

The Langmuir probe was used for the detection of the negative hydrogen ions H^- by means of the method described by Amemiya [10], but this research found no peak related to the negative ions in the second derivative of the probe characteristics. According to [11], this result is not a proof of the absence of the negative ions in the plasma.

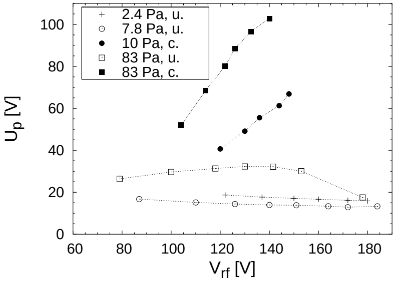

Figure 3.5: *The plasma potential (U_p) as a function of the voltage delivered to the powered electrode (V_{rf}). The open symbols represent the unconfined mode, the closed symbols represent the confined mode.*

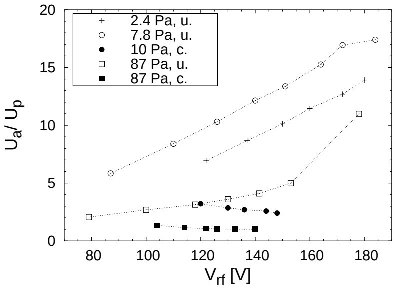

Figure 3.6: *The ratio (U_a/U_p) as a function of the voltage delivered to the powered electrode (V_{rf}). The open symbols represent the unconfined mode, the closed symbols represent the confined mode.*

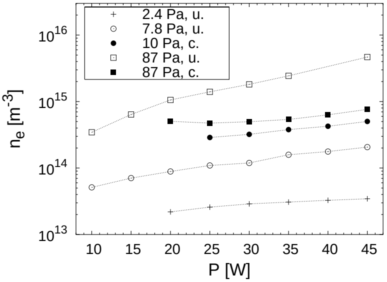

Figure 3.7: *The electron concentration as a function of the RF power (P). The open symbols represent the unconfined mode, the closed symbols represent the confined mode.*

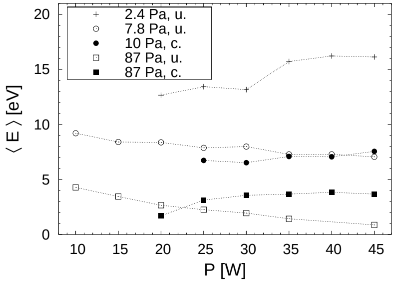

Figure 3.8: *The mean electron energy as a function of the RF power (P). The open symbols represent the unconfined mode, the closed symbols represent the confined mode.*

3.3 Modelling of the plasma potential

Efforts were made to find an explanation for the existence of the two modes by means of a simple capacitive model [12], that among others gives the equation

$$U_p = \frac{C_a}{C_a + C_g} V_{rf} \tag{3.1}$$

(U_p is the plasma potential, V_{rf} the amplitude of the RF voltage on the powered electrode, C_a the capacity of the sheath at the powered electrode and C_g the capacity of the sheath between the plasma and the grounded reactor parts). The capacities of the sheaths at the electrodes were calculated as capacities of planar capacitors. For the calculation of the sheath thicknesses it was assumed that the ion concentration in the sheaths is constant and the electron concentration in the sheaths is zero. The capacity of the sheath between plasma and the grounded reactor wall was calculated as the capacity of a spherical capacitor. These led to

$$C_a = A_a \sqrt{\frac{\varepsilon_0 e n_e (C_a + C_g)}{2 C_g V_{rf}}} \tag{3.2}$$

$$C_g = \frac{4\pi\varepsilon_0}{\frac{1}{R'} - \frac{1}{R}} + A_a \sqrt{\frac{\varepsilon_0 e n_e (C_a + C_g)}{2 C_a V_{rf}}} \tag{3.3}$$

(A_a is the area of the powered electrode, ε_0 the vacuum permittivity, e the elementary charge, R the inner radius of the reactor and $R - R'$ the thickness of the sheath at the reactor wall. The value of R was chosen to be 125 mm.)

When the changes in the ion drift velocity are neglected, the ion concentration n_i in the distance r from the reactor centre is in the (collisional) spherical sheath at the reactor wall approximately given by

$$n_i(r) = n_e \left(\frac{R'}{r}\right)^2 \tag{3.4}$$

Solving the Poisson equation with this ion concentration dependence leads to

$$\frac{C_1}{C_1 + C_2} \frac{V_{rf}}{n} = \frac{e R'^2}{\varepsilon_0} \left(\ln \frac{R}{R'} + \frac{R'}{R} - 1\right) \tag{3.5}$$

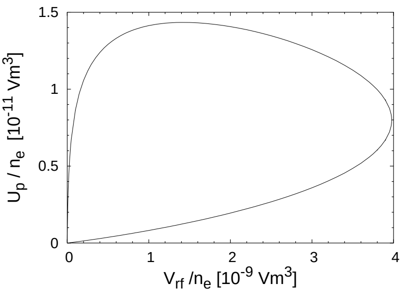

Figure 3.9: *The solution of the equations (3.2), (3.3) and (3.5): The dependence of the ratio U_p/n_e on the parameter V_{rf}/n_e.*

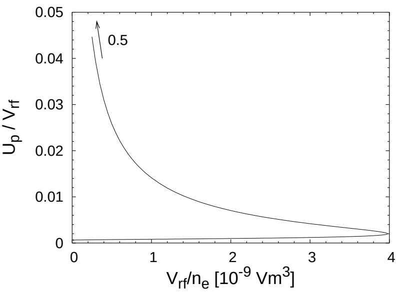

Figure 3.10: *The solution of the equations (3.2), (3.3) and (3.5): The dependence of the ratio U_p/V_{rf} on the parameter V_{rf}/n_e.*

The left side of the eq. (3.5) is equal to the plasma potential divided by the electron concentration.

There are three unknown quantities (C_1, C_2 and R') in the three equations (3.2), (3.3) and (3.5) that depend on the ratio V_{rf}/n_e and can be numerically solved. The three given equations have two possible solutions under a critical value of the ratio V_{rf}/n_e. This can be seen in figs. 3.9 and 3.10 where the dependences of the plasma potential divided by the electron concentration (U_p/n_e) and by the RF amplitude (U_p/V_{rf}), respectively, on the ratio V_{rf}/n_e are shown.

The lower branch in the graphs is related to the unconfined mode. Due to the plasma spreading from the interelectrode space towards the reactor walls the capacity C_g is high compared to C_a. This leads to the low plasma potential which retrospectively enables the plasma spreading to the grounded reactor parts.

In the upper branch of the plots in figs. 3.9 and 3.10 related to the confined mode the value of plasma potential is relatively high. The electric field repels the electrons from the grounded objects and does not allow the spreading of the plasma from the interelectrode space. This is the reason for the low value of the capacity C_g, which keeps the plasma potential relatively high according to eq. (3.1). The capacity C_g is comparable to the capacity C_a and therefore, the voltage drops, at the driven and at the grounded electrode, are also comparable. In the limit case when the ratio $V_{rf}/n_e \rightarrow 0$ the plasma potential almost reaches the value $V_{rf}/2$. According to eq. (3.1) this is possible only when $C_a \approx C_g$ i.e. when the influence of the first term on the left side of the eq. (3.3) is negligible.

Although the model explains well the existence of the two observed modes, it does not give quantitatively true values of the plasma potential. The model approximations limiting its usage are especially the simplifications of the electrical properties of the sheaths and the bulk plasma, the neglect of the thermal electron energy and the simplification of the reactor and glow geometry. For further details see ref. [13].

As the simple model, described above, gives good results, I decided to search for a more general model with more reliable input equations. A starting point was the equation $U_a/U_p = [(A_a + f(R'))/A_a]^{\alpha}$ (see [6, 7, 8]), where $f(R')$ is a positive growing function representing the influence of the grounded reactor parts, therefore the term $A_a + f(R')$ represents an effective area of the grounded electrode. Since the DC voltage on a sheath is directly proportional to the RF sheath voltage [14], I can write $U_p + U_a = \beta V_{rf}$ and

$$U_p = \frac{\beta V_{rf}}{1 + \left[1 + \frac{f(R')}{A_a}\right]^{\alpha}} \tag{3.6}$$

The advantage of the model is that its qualitative behaviour is valid for any value of the constants $\alpha, \beta > 0$.

The second equation of the model was obtained by solving the Poisson equation in the sheath at a grounded part of the reactor. Assuming spherical sheath with positive charge density $\rho = en_e\,(R'/r)^{\gamma}$ and $\gamma > 0$ we obtain values of the plasma potential that are shown in the fig. 3.11. The change of the sheath geometry (e.g. to planar sheath) does not change the shape of the plotted curve significantly.

Since the right side of the eq. (3.6) is in the whole range $0 \leq R' \leq R$ a positive and decreasing function of R', there are two intersections of the equation (3.6) and the curve in the fig. 3.11 or there is no intersection. The two intersections correspond to the two solutions of the simple model described above and the two models are in agreement.

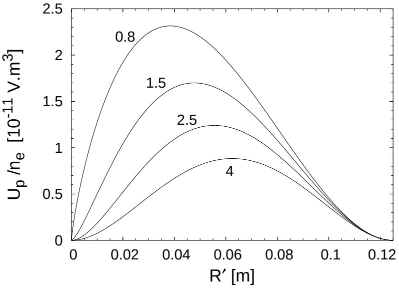

Figure 3.11: *Plasma potential calculated by means of the Poisson equation for γ = 0.8, 1.5, 2.5 and 4.*

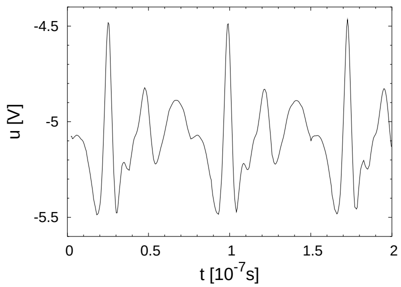

Figure 3.12: *Voltage measured by the uncompensated probe in the discharge centre at 9.95 Pa in the unconfined mode.*

3.4 Frequency spectrum of the plasma potential

The importance of the frequency spectrum measurements is demonstrated in the fig. 3.12, where is shown an example of the voltage measured by the uncompensated probe. The figure shows that the amplitudes of the higher harmonics were not negligible.

Initially a description of the behaviour of the fundamental frequency (13.56 MHz). When measured as a function of pressure, its amplitude (V_1) was correlated with the plasma potential. The measurements of the spatial distribution of the fundamental harmonic showed (fig. 3.13) that its amplitude changed strongly in the sheaths and it was more or less constant in the bulk plasma. There were no important differences between the amplitudes V_1 in the confined and in the unconfined mode, only the change in the sheath thicknesses can be clearly seen in the fig. 3.13.

It is worth noting that the bulk plasma impedance was not negligible at the low pressure 2.44 Pa, therefore there were significant changes of the amplitude V_1 in the bulk plasma (see fig. 3.14). This was caused by the low electron concentration. In contrast to the measurements published by Dyson at al. [15] no observation was made of any change in the sign of

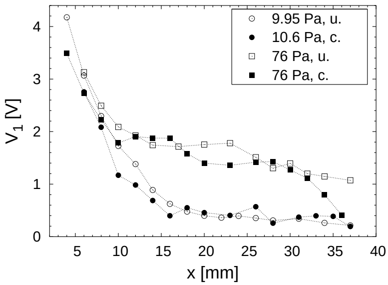

Figure 3.13: *The amplitude of the fundamental harmonic in different distances from the powered electrode (x). The open symbols represent the unconfined mode, the closed symbols represent the confined mode.*

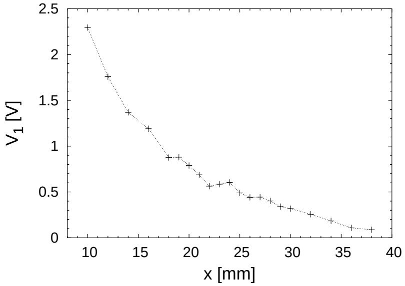

Figure 3.14: *The amplitude of the fundamental harmonic in different distances from the powered electrode (x) at the pressure 2.44 Pa.*

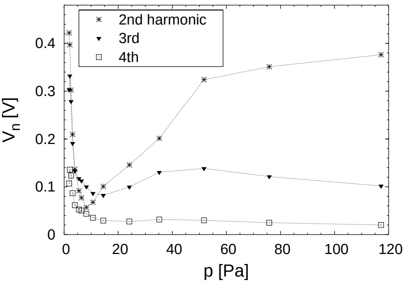

Figure 3.15: *The amplitudes of a few higher harmonics as functions of the pressure.*

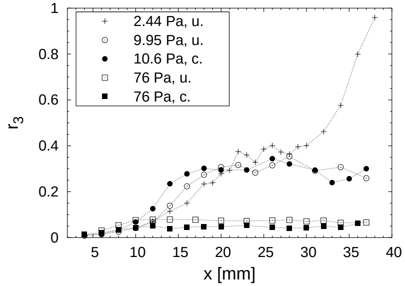

Figure 3.16: *The relative amplitude of the 3^{rd} harmonic in different distances from the powered electrode.*

the derivation $\mathrm{d}V_1/\mathrm{d}x$ at the plasma-sheath boundary. Dyson observed this change at low pressure due to the capacitive character of the sheath and the inductive character of the bulk plasma. In this experiment the electron energy in the low pressure was so high, that the electrons penetrated into the sheath and changed its character from the capacitive to the inductive (see sect. 3.2 and fig. 3.3).

The amplitudes of a few higher harmonics as functions of pressure are shown in the fig. 3.15. The series plasma-sheath resonances [16, 17, 18] of the higher harmonics were detected at low pressure (under 3 Pa). Also the spatially resolved measurements of the higher harmonics were carried out and it was shown, that their amplitudes grew linearly and quickly in the sheaths whereas in the bulk plasma their changes were relatively slow. An example is drawn in the fig. 3.16, where the relative amplitude of the third harmonic (r_3) is shown. The relative amplitude r_3 is the amplitude of the third harmonic divided by the fundamental harmonic amplitude.

A series of measurements focused on the higher harmonics were carried out and the dependence of their amplitudes on pressure, power, discharge regime and position was studied. Further it was observed the behaviour of the harmonics in the mixtures of hydrogen and argon, nitrogen or oxygen. It was proved that the intensity of higher harmonics is not a simple function of the DC sheath voltages and it also depends on other plasma parameters (probably electron concentration or energy).

3.5 Reference probe

The reference probe is above all used for the correction of the Langmuir probe characteristic [2], that can be critically disturbed by the changes of the plasma potential caused by the current flowing to the Langmuir probe [19]. The reference probe located near the Langmuir probe measures therefore the floating potential (U_{ref}), that depends on the Langmuir probe current (I), eventually on the Langmuir probe voltage (U). Kleber and Overzet [2] demonstrated, that when the Langmuir probe potential is significantly lower than the plasma potential (U_p), the reference probe potential is given by the equation $U_{ref} = U_{ref\,0} + R_{sh}.I$, where R_{sh} is called the sheath resistance.

The examples of the measured functions $U_{ref}(I)$ and $U_{ref}(U)$ are shown in the figures 3.17 and 3.18. I found that for $U \leq u_p$, where u_p is the actual value of the plasma potential influenced by the Langmuir probe, the

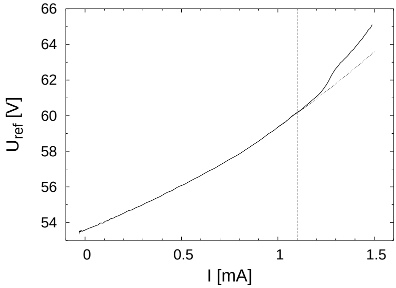

Figure 3.17: *The reference probe voltage as a function of the Langmuir probe current. The vertical line denotes the current flowing to the Langmuir probe when $U = u_p$. The dotted line represents the polynomial (3.7).*

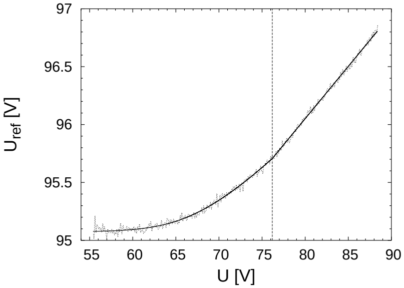

Figure 3.18: *The reference probe voltage as a function of the Langmuir probe voltage. The vertical line denotes the point when $U = u_p$. The solid line represents the model (3.8)–(3.11).*

reference probe potential can be written in the form

$$U_{ref} = U_{ref\,0} + R_{sh}(I).I = P^p(I) \tag{3.7}$$

where $P^p(I)$ is a polynomial of a low degree p. In my measurements the maximal value of p was three. The nonlinearity of the sheath for the DC current was proved, i.e. the sheath resistance depended on the current I. By means of the correlation analysis it was found, that this "DC" nonlinearity strongly depended on the Langmuir probe current and was not significantly influenced by the sheath parameters.

In some cases the dependence $U_{ref}(I)$ for $U > u_p$ was relatively complicated when compared to the polynomial (3.7), but it was observed as a linear dependence $U_{ref}(U)$ for $U > u_p$. Therefore a simple model was used for the dependence $U_{ref}(U)$ that could be useful for estimation of the plasma parameters. The model equations are

$$u_p = U_p + A\,\mathrm{e}^{-\frac{u_p - U}{kT_e}} \qquad \text{for}\, U \le u_p \tag{3.8}$$

$$u_p = aU + b \qquad \text{for}\, U \ge u_p \tag{3.9}$$

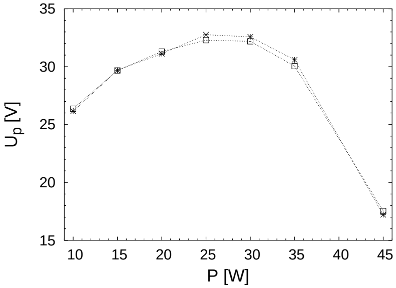

Figure 3.19: *The comparison of the plasma potential obtained by means of the Langmuir probe (□) and by means of the model (3.8)–(3.11) (∗). Measured at 86 Pa for different values of the RF power (P).*

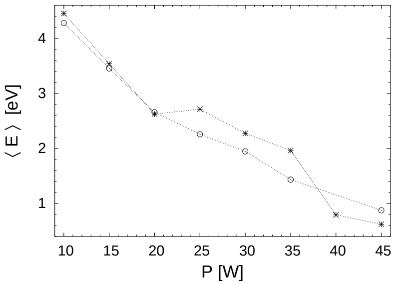

Figure 3.20: *The comparison of the mean electron energy obtained by means of the Langmuir probe (□) and by means of the model (3.8)–(3.11) (∗). Measured at 86 Pa for different values of the RF power.*

$$
\begin{aligned}
U_{ref} &= \alpha u_p + \beta && (3.10)\\
b &= (U_p + A)(1 - a) && (3.11)
\end{aligned}
$$

where T_e is the electron temperature and k the Boltzmann constant. The parameters of the model (U_p, A, T_e, α, β, a) can be obtained numerically, but the numerical procedure must be carried out carefully since it is error-prone. For large Langmuir probes a very rough approximation $U_p = (U_{ref\,0} - \beta)/\alpha$ for the plasma potential estimation can be used, that avoids the numerical procedure mentioned above.

The comparison of the plasma parameters obtained by means of the model (3.8)–(3.11) and by the Langmuir probe are shown in the fig. 3.19 and 3.20. The model was relatively successful, especially in the estimation of the plasma potential. The validity of the model was restricted to the conditions, when the nonlinear behaviour of the dependence $U_{ref}(I)$ was reached, but it did not seem to be restricted to the bulk plasma. Therefore the presented model can be in some cases used for approximate estimation of the plasma parameters in the sheaths, where the Langmuir probe does not usually give any meaningful results.

3.6 Ion energy distributions

The amount and energy of ions impinging on a solid surface plays a crucial role in many plasma applications, therefore it is important to know the IEDs. The dominating ions in the discharge were H_3^+ produced mainly by the reaction

$$H_2^+ + H_2 \rightarrow H_3^+ + H. \tag{3.12}$$

Their distribution function was relatively simple with a saddle structure and a tail rapidly decreasing towards lower energies (see fig. 3.21). The IED of H_2^+ had many peaks in the whole spectrum so that the saddle structure could not be exactly distinguished (see fig. 3.22). This complicated structure resulted from a charge transfer reaction having a relatively large cross section [20, 21]. The ion with the lowest concentration was H^+. Its distribution function had a well developed broad saddle structure (see fig. 3.23) caused by its low mass [22]. No clusters with more than three hydrogen atoms were observed.

It is interesting to discuss the origin of the high-energy tail in the H^+ energy distribution. It can be seen from fig. 3.23 that some H^+ ions have kinetic energy more than 10 eV higher than the high-energy part of the saddle structure. The presence of the H^+ ions with such a high energy can be explained by a dissociative ionization of the H_2 molecules by electron impact via the repulsive ${}^2\Sigma_u^+$ state of the H_2^+ [23]. This process requires electrons with energy over 30 eV and produces H^+ ions with the energy observed. The presence of the required high-energy electrons was demonstrated by means of the Langmuir probe (sect. 3.2).

The IEDs of the H_3^+, H_2^+ and H^+ ions for different vertical distances from the RF electrode are shown in fig. 3.21, 3.22 and 3.23, respectively. Their concentrations decreased significantly in the above given ion sequence. Therefore, the IEDs had to be measured with different voltages on the secondary electron multiplier and the absolute values in the figures can not be compared. The integrals of the IEDs depending on the distance from the RF electrode are shown in fig. 3.24. The structure of the IEDs and their integrals did not change strongly while moving the PPM extraction orifice along the glow region (approximate position range 23–38 mm). The width of the saddle structure was slightly reduced when the PPM moved towards the grounded electrode. This is a result of decreasing RF voltage amplitude when moving from the sheath edge at the RF electrode to the grounded one. This is in accord with the results presented in sect. 3.4.

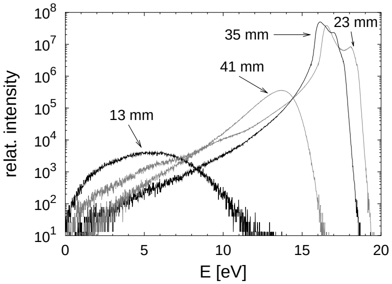

Figure 3.21: *IED of H_3^+ in different vertical distances from the RF electrode for 2.42 Pa and 30 W*

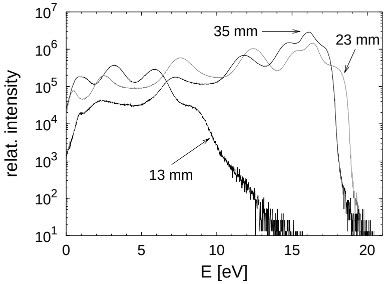

Figure 3.22: *IED of H_2^+ in different vertical distances from the RF electrode for 2.42 Pa and 30 W*

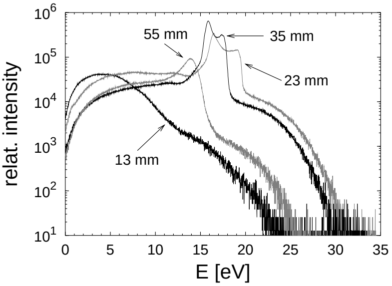

Figure 3.23: *IED of H^+ in different vertical distances from the RF electrode for 2.42 Pa and 30 W*

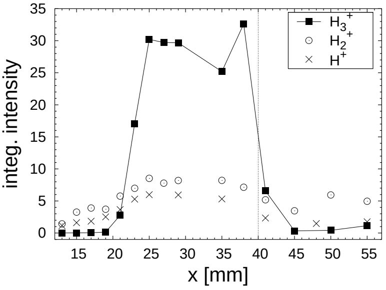

Figure 3.24: *Integrals of the IEDs of H^+, H_2^+ and H_3^+ in different vertical distances from the RF electrode. 40 mm is the position of the grounded electrode.*

The IEDs and their integrals exhibited strong variations concerning the spatial changes along the sheath at the RF electrode (see fig. 3.21–3.24 for the position below 23 mm). The IED integrals outside the glow region were rapidly decreasing, especially for H_3^+. This can be explained by a decrease of the ion concentration in the sheath as well as by the fact that the positive ions are attracted rather to the RF electrode than to the grounded extraction hood.

Compared to the RF electrode the sheath at the grounded electrode was very thin due to the discharge asymmetry mentioned in the sections 3.2 and 3.3. Therefore, the spatially resolved IEDs along this sheath could not be measured. The IEDs integrals and simultaneously the mean ion energy decreased at the position close to the grounded electrode. A detectable concentration of the ions was detected even below the grounded electrode in accord with ref. [24].

The effect of pressure and RF power on the IEDs was also studied for a fixed position at the glow region. For further details concerning this section see [25].

3.7 Optical emission spectroscopy

The optical emission spectroscopy enables the calculation of the dissociation degree of the hydrogen molecules. This method is based on the the comparison of the atomic (Balmer α) line intensity ($I_{H\alpha}$) and the molecular line (Fulcher – $3d^3\Pi_u^- \rightarrow 2a^3\Sigma_g^+$, 2-2, Q1) intensity ($I_{Q1}$) [26]. The dissociation degree was calculated only in the case of sufficiently low pressure, where the results cannot be influenced by the collisions of excited particles. For high pressure only the ratio $I_{H\alpha}/I_{Q1}$ is published, that is a rough measure of the dissociation degree behaviour (see fig. 3.26).

The value of the dissociation degree was between 0.3 and 0.5. It was observed that the dissociation degree slightly decreases when the hydrogen pressure increases (fig. 3.25). According to approximate calculations, the dissociation rate constant steeply decreases by increasing pressure due to the fall of the electron energy. Therefore the decrease of the dissociation degree can be accredited to the influence of the electron energy (sect. 3.2).

Fig. 3.25 and 3.26 show that the dissociation degree is strongly reduced by the transition from the unconfined to the confined mode. By the mode transition the values of the electron concentration and energy in the dis-

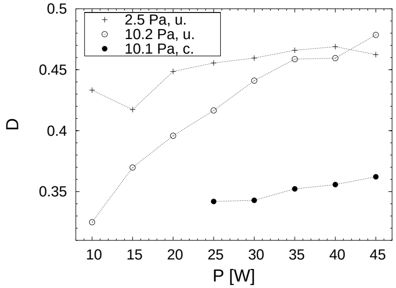

Figure 3.25: *Dissociation degree (D) as a function of the RF power. The open symbols represent the unconfined mode, the closed symbols represent the confined mode.*

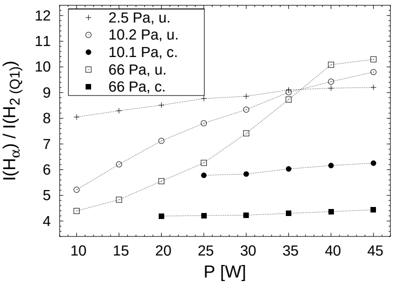

Figure 3.26: *The ratio $I_{H\alpha}/I_{Q1}$ as a function of the RF power. The open symbols represent the unconfined mode, the closed symbols represent the confined mode.*

charge centre were not changed in that way, that could explain the sharp decrease of the dissociation degree. This means that an important part of the hydrogen molecules was dissociated in the sheaths, because the mode transition influenced above all the sheath characters. The sheath at the grounded electrode was enlarged and the sheath at the powered electrode was reduced by the transition. Since the dissociation degree decreased by the transition, it can be deduced that the sheath at the powered electrode had higher impact on the dissociation than the sheath at the grounded electrode. Taking into account the high value of the ratio U_a/U_p (see sect. 3.2) this result is not surprising.

The optical emission spectroscopy also enables the measurement of discharge temperatures. The excitation temperature of the hydrogen atoms (fig. 3.27) was correlated with the electron temperature. In contrast the rotational temperature of hydrogen molecules in the ground state (fig. 3.28) was an increasing function of pressure. A simple explanation for the rotational temperature growth is the increasing efficiency of the collisional processes that transform the energy of excited particles and ions to the translational and rotational energy of the neutral gas.

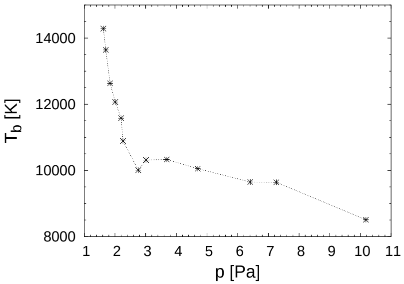

Figure 3.27: *The excitation temperature of hydrogen atoms (T_b) as a function of pressure.*

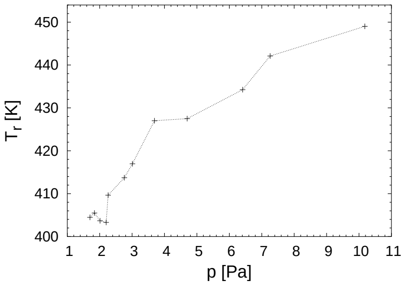

Figure 3.28: *The rotational temperature (T_r) as a function of pressure.*

Chapter 4

Conclusion

The main object of this work was the diagnostics of the low-pressure, high-frequency, capacitively coupled hydrogen plasma. The experiments were carried out in a spherical stainless steel reactor with two horizontally mounted, parallel, stainless steel electrodes of 80 mm in diameter. The upper electrode, embedded in a grounded ring, was driven at the frequency of 13.56 MHz. The bottom electrode was grounded. For diagnostic purposes I used the RF compensated Langmuir probe with a reference probe, an uncompensated potential probe, a positive ion mass and energy spectrometer (PPM 421 Balzers) and the optical emission spectroscopy. I calculated the energy-dependent transmission function of the entry ion optics of the PPM.

Two regimes of discharge were studied. They differed mainly in the plasma potential, the DC voltage between the plasma and the powered electrode, the discharge asymmetry and the visual appearance of the discharge. The abrupt transition between the regimes was induced by a change of the gas pressure or the RF power and it showed a hysteresis. The existence of the two regimes and their basic properties were explained by means of well-known equations, that describe the sheaths in capacitively coupled discharges.

The nonlinearity of the sheath for DC current was proved, i.e. the sheath resistance depended on the DC current flowing through the sheath. The nonlinearity depended mainly on the DC current, the parameters of the sheath did not influence this nonlinearity significantly. It was shown, that the nonlinear behaviour can be used in some cases for the approximate evaluation of the plasma parameters, especially in the sheaths, where the interpretation of the Langmuir probe measurements is not reliable.

This work shows the dependences of the plasma parameters describing the hydrogen capacitively coupled discharge on the gas pressure, the position in the discharge and the RF power. It marginally concerns the problems of the admixtures of Ar, N_2 and O_2.

At low pressure there was observed a thin, intensively radiating layer at the plasma-sheath boundary at the RF electrode. In this layer the electron concentration and temperature had sharp maxima. Among the detected ions (H_3^+, H_2^+, H^+) there was a group of fast H^+ ions with kinetic energy approx. 10 eV higher than the maximum value of the energy gained in the sheath. The presence of this group was explained by the dissociative ionisation of molecules H_2 via the repulsive state ${}^2\Sigma_u^+$, that was activated by high-energy electrons.

Further, the frequency spectrum of the plasma potential, the shape of the EED and its most important moments, the temperatures characterizing the plasma, the dissociation degree of the hydrogen molecules and other subjects were studied.

The thesis brings and partly explains some findings about the low-pressure hydrogen capacitively coupled discharges and I hope that it can serve as a starting point for further research, e.g. in the field of hydrogen discharges with admixtures or the fourier spectrum of the plasma potential.

Bibliography

[1] M. B. Hopkins. Langmuir probe measurements in the gaseous elecronics conference RF reference cell. *Journal of Research of the National Institute of Standards and Technology*, **100**: 415–425, 1995.

[2] J. L. Kleber and L. J. Overzet. Sheath resistance measurements in the GEC reference reactor. *Plasma Sources Science & Technology*, **8**: 534–543, 1999.

[3] P. Dvořák. Diagnostika reaktivního plazmatu, snaha o pochopení procesu plazmochemické depozice. Master's thesis, Přírodovědecká Fakulta Masarykovy Univerzity v Brně, 2001.

[4] Zajíčková L., Dvořák P., Kudrle V., and Šmíd R. Study of mode transition in low pressure capacitive rf discharges in nitrogen. *Czechoslovak Journal of Physics*, **52**: 427–432, 2002.

[5] Y. P. Song, D. Field, and D. F. Klemperer. Electrical potentials in rf discharges. *Journal of Physics D: Applied Physics*, **23**: 673–681, 1990.

[6] M. A. Lieberman. Spherical-shell model of an asymmetric rf discharge. *Journal of Applied Physics*, **65**: 4186–4191, 1989.

[7] M. A. Lieberman and S. E. Savas. Bias voltage in finite length, cylindrical and coaxial radio-frequency discharges. *Journal of Vacuum Science & Technology A – Vacuum Surfaces and Films*, **8**: 1632–1641, 1990.

[8] M. A. Lieberman and A. J. Lichtenberg. *Principles of plasma discharges and materials processing.* John Wiley & sons, inc., New Plasma Sources SciYork, 1994.

[9] M. A. Sobolewsli. Electrical characteristics of argon radio frequency glow discharges in an asymmetric cell. *IEEE Transactions on Plasma Science*, **23**: 1006–1022, 1995.

[10] H. Amemiya and Y. Sakamoto. Negative ions and energy distribution in a hydrogen plasma device. *Japanese Journal of Applied Physics*, **26**: 1170–1178, 1987.

[11] Vucelić M. and Mijović S. Information from probe characteristics in negative ion containing plasma. *Journal of Applied Physics*, **84**: 4731–4735, 1998.

[12] Snijkers R. J. M. M. *The sheath of an RF plasma: measurements and simulations of the ion energy distribution.* PhD thesis, Technische Univesiteit Eindhoven, 1993.

[13] P. Dvořák, L. Zajíčková, and J. Janča. Plasma potential in low-pressure capacitive r.f. discharges. In *WDS'03 - Proceedings of Contributed Papers - Part II*, 2003.

[14] M. A. Lieberman. Analytical solution for capacitive rf sheath. *IEEE Transactions on Plasma Science*, **16**: 638–644, 1988.

[15] A. Dyson and J. E. Allen. Field probe for low-pressure capacitively coupled radio-frequency discharge plasmas. *Measurement Science and Technology*, **14**: 107–113, 2003.

[16] B. M. Annaratone, V. P. T. Ku, and J. E. Allen. Identification of plasma–sheath resonances in a parallel–plate plasma reactor. *Journal of Applied Physics*, **77**: 5455–5457, 1995.

[17] V. P. T. Ku, B. M. Annaratone, and J. E. Allen. Plasma–sheath resonances and energy absorption phenomena in capacitively coupled radio frequency plasmas. Part I. *Journal of Applied Physics*, **84**: 6536–6545, 1998.

[18] V. P. T. Ku, B. M. Annaratone, and J. E. Allen. Plasma–sheath resonances and energy absorption phenomena in capacitively coupled radio frequency plasmas. Part II. *Journal of Applied Physics*, **84**: 6546–6551, 1998.

[19] V. A. Godyak, R. B. Piejak, and B. M. Alexandrovich. Measurements of electron energy distribution in low-pressure rf discharges. *ence & Technology*, **1**: 36–58, 1992.

[20] T. Šimko. *Modélisation du transport ionique et électronique dans un gaz soumis à un champ électrique. Comparaison modèle-experience pour l'hydrogène.* PhD thesis, Université de Paris-sud, 1997.

[21] P. W. May, D. Field, and D. F. Klemperer. Modeling radio-frequency discharges: Effect of collisions upon ion and neutral particle energy distributions. *Journal of Applied Physics*, **71**: 3721–3730, 1992.

[22] D. Field, D. F. Klemperer, P. W. May, and Y. P. Song. Ion energy distributions in radio-frequency discharges. *Journal of Applied Physics*, **70**: 82–92, 1991.

[23] R. K. Janev, D. Reiter, and U. Samm. *Collision Processes in Low-Temperature Hydrogen Plasmas.* Forschungszentrum Jülich, Jülich, 2003.

[24] R. Šmíd, L. Zajíčková, and J. Janča. Spatially resolved measurements in r.f. capacitive discharges in argon and nitrogen. *Czechoslovak Journal of Physics – Suppl. C*, **54**: 592–598, 2004.

[25] P. Dvořák, J. Jánský, L. Zajíčková, and J. Janča. Energy distribution of hydrogen ions in capacitively coupled low pressure discharge. *Acta Physica Slovaca*, **55**: 441–446, 2005.

[26] Lang N., Lavrov B. P., and Röpcke J. Spectroscopic determination of the dissociation degree in pulsed plasmas containing hydrogen. In *Proceedings of Frontiers in Low Temperature Plasma Diagnostics IV*, 2001.